HHS Public Access

Author manuscript

J Mod Opt. Author manuscript; available in PMC 2017 November 09.

Published in final edited form as:

J Mod Opt. 2017 ; 64(17): 1800–1807. doi:10.1080/09500340.2017.1318966.

Enhancement of intrinsic optical signal recording with split spectrum optical coherence tomography

Damber Thapa[a], **Benquan Wang**[a], **Yiming Lu**[a], **Taeyoon Son**[a], and **Xincheng Yao**[a,b]

[a]Department of Bioengineering, University of Illinois at Chicago, Chicago, IL, USA

[b]Department of Ophthalmology and Visual Sciences, University of Illinois at Chicago, Chicago, IL, USA

Abstract

Functional optical coherence tomography (OCT) of stimulus-evoked intrinsic optical signal (IOS) promises to be a new methodology for high-resolution mapping of retinal neural dysfunctions. However, its practical applications for non-invasive examination of retinal function have been hindered by the low signal-to-noise ratio (SNR) and small magnitude of IOSs. Split spectrum amplitude-decorrelation has been demonstrated to improve the image quality of OCT angiography. In this study, we exploited split spectrum strategy to improve the sensitivity of IOS recording. The full OCT spectrum was split into multiple spectral bands and IOSs from each sub-band were calculated separately and then combined to generate a single IOS image sequence. The algorithm was tested on *in vivo* images of frog retinas. It significantly improved both IOS magnitude and SNR, which are essential for practical applications of functional IOS imaging.

Keywords

Optical coherence tomography; intrinsic optical signals; split spectrum; functional imaging of retina; ophthalmology

1. Introduction

Electrophysiological techniques such as electroretinography (ERG) (1, 2) are traditional methods for objective evaluation of retinal physiology. However, the spatial resolution of ERG measurements is limited. Stimulus-evoked intrinsic optical signal (IOS) changes promise a high-resolution alternative to electrophysiological assessment of retinal physiology (3). Comparative IOS imaging of wild-type and mutant mouse retinas has revealed IOS distortion associated with retinal disease (4). It is known that major eye diseases, such as retinitis pigmentosa, age-related macular degeneration, glaucoma and diabetic retinopathy, primarily affect specific cell types of the retina. Therefore, high-resolution IOS imaging holds unparalleled advantages over traditional electrophysiological methods. By providing excellent axial resolution, optical coherence tomography (OCT) has

CONTACT. Xincheng Yao, xcy@uic.edu.

Disclosure statement

No potential conflict of interest was reported by the authors.

been explored to conduct depth-resolved IOS imaging of retinal activity (5–8). To date, functional OCT has been used to detect IOSs in frog (5, 9, 10), mouse (4, 11), rat (8), rabbit (6), chicken (12, 13), macaque (14) and human (15) retinas. Yao et al. used a time-domain OCT (TD-OCT) to record IOSs from the photoreceptor and ganglion cell layers in isolated frog retinas (5). Bizheva et al. detected IOSs in photoreceptor inner/outer segments and plexiform layers in isolated rabbit retinas (6). Srinivasan et al. used a spectral-domain OCT (SD-OCT) to demonstrate IOSs in live rat retinas (8). Suzuki et al. mapped positive IOS (intensity of OCT signal increased) in the outer segment (OS) and negative IOS (intensity of OCT signal decreased) in the inner segment ellipsoid (ISe) in macaque retinas (14). The stimulus-evoked IOSs in human retinas was first demonstrated by Srinivasan et al. (15) using ultrahigh resolution SD-OCT and later by Hillmann et al. (16) using parallelized and computationally aberration-corrected swept source OCT. Recently, Zhang et al. recorded IOSs in the photoreceptor and inner layers of *in vivo* images of frog retinas at the subcellular resolution (9). Transient IOSs were consistently observed in the photoreceptor layer almost immediately (<4 ms) after the stimulation. In contrast, relatively slow IOS changes were observed in the inner retina.

The IOS imaging promises a new methodology for high-resolution mapping of retinal neural dysfunctions (3). However, its practical applications for non-invasive examination of retinal function have been hindered by the low signal-to-noise ratio (SNR) and small magnitude of IOSs. To ensure the reliable SNR of IOS measurement, multiple measurements from the same location are typically required for average, which limited its application for clinical applications due to inevitable eye motions during continuous and long-term measurements (9). Also, reliable recording of fast IOSs that have time courses comparable to retinal electrophysiological kinetics is still challenging because of limited SNR (9). Recently, split spectrum amplitude-decorrelation has been demonstrated to improve the image quality of OCT angiography (17). In this paper, we exploit split spectrum strategy to enhance the sensitivity of IOS recording in different layers of live frog retina. We calculate IOSs from B-scans of each sub-bands separately and then fused to single topographical maps. Compared to the full spectrum OCT, split spectrum OCT significantly increased SNR, number of activated pixels and IOS magnitude.

2. Materials and methods

2.1. IOS calculation

The experimental data were retrieved from our previous study that validated physiological assessment of retinal rod and cone photoreceptors in live frog eye using SD-OCT (9). The SD-OCT consisted of a broadband superluminescent diode (SLD; Superlum Ltd., Ireland) with a center wavelength of 846 nm and full width at half maximum (FWHM, $\Delta\lambda$) of 104 nm. For functional IOS imaging, OCT recording consists of stacks of B-scans before the stimulation (pre-stimulus), during the stimulation and after the stimulation (post-stimulation). B-scan images are usually registered to compensate for eye movements before IOS calculations. The IOS of each pixel is calculated as (18, 19)

$$\mathrm{IOS}(x,z,t)=\frac{I(x,z,t)-\overline{I}(x,z)}{\overline{I}(x,z)} \quad (1)$$

where $I(x, z, t)$ is the intensity of a pixel at transverse position x, retinal depth z and time t. $\bar{I}(x, z)$ is the average intensity of the pixels from all the B-scans captured in the pre-stimulation phase at retinal location (x, z). A positive or negative IOS corresponds to the stimulus-evoked increase or decrease in the OCT intensity, respectively. To increase the SNR, an appropriate threshold was selected to reject background noise, and to define the stimulus-evoked positive and negative IOSs as follows (9).

$$I(x,z,t)>\overline{I}(x,z)+3\sigma(x,z) \quad (2)$$

$$I(x,z,t)<\overline{I}(x,z)-3\sigma(x,z) \quad (3)$$

where $\sigma(x, z)$ is the standard deviation of intensity at pixel location (x, z) from B-scans captured before stimulation. The absolute activated pixels are the pixels which have either positive, negative or both activated pixels.

2.2. IOS with split spectrum OCT

According to basic OCT theory, spectral interference signal recorded by SD-OCT, after auto-correlation and DC terms ignored, can be simply given by (17)

$$I(k)=\int_{-\infty}^{\infty} R(k)E(k,z)\ \cos(2\mathrm{kz})\,\mathrm{d}z \quad (4)$$

where k is the wave number, $I(k)$ is the interferometric spectra obtained by interference between the light reflected from the reference mirror $R(k)$ and the light reflected from the sample $E(k, z)$, z is the optical delay between the light reflected from the reference mirror and the sample. The measured interferometric spectra are transformed to the k-space through a re-sampling procedure (20). The complex amplitude of OCT signal, usually referred A-scan $I(z)$, can be obtained from the inverse Fourier transform of $I(k)$.

$$I(z)=\mathrm{FFT}[I(k)] \quad (5)$$

OCT B-scan images were reconstructed from the amplitude of the acquired OCT spectrums $|I(z)|$. The B-scans acquired from the full spectrum OCT were used to create IOS images as described in Section 2.1. In this study, we divide the full OCT spectrum $I(k)$ into four spectral bands by using Gaussian filters. The individual sub-spectrums were then passed into

the conventional Fourier transform separately to achieve OCT signals from each spectral band as

$$S_1(z)=\mathrm{FFT}[I(k)G_1(n)]$$

$$S_2(z)=\mathrm{FFT}[I(k)G_2(n)]$$

$$S_3(z)=\mathrm{FFT}[I(k)G_3(n)]$$

$$S_4(z)=\mathrm{FFT}[I(k)G_4(n)] \quad (6)$$

where $S_1(z)$, $S_2(z)$,…, $S_4(z)$ are OCT signals from spectral bands 1, 2, …, 4, respectively. $G_i(n)$ is the Gaussian filter whose function is given by

$$G_i(n)=\exp\left[-\frac{(n-m)^2}{2c^2}\right] \quad (7)$$

where n is the spectral element number that is linearly mapped with the wavenumber (k), m is the position of the spectral peak and c is the standard deviation. The sub-bands overlap and comprise spectral elements, corresponding to the full width at half maximum (FWHM, $\Delta\lambda$) of 41 nm. After passing individual split spectrums into conventional Fourier transform, B-scans were reconstructed from each spectral band separately. Adjacent B-scans within each spectral band were then registered to compensate for eye movements before IOS calculations. Details about this registration process can be found in our previous publication (9). Successively, IOS images were calculated from each spectral band separately. IOSs from the full OCT spectrum and split OCT spectrum are compared at different retinal layers by matching IOS magnitudes and SNRs from different layers of retina. IOS signals over certain depth range were averaged to create a signal at each retinal layer. The SNR is calculated by

$$\mathrm{SNR}=\frac{I(t)}{\sigma} \quad (8)$$

where $I(t)$ is the IOS signal after t sec of stimulation and σ is the standard deviation of IOS signal in the pre-stimulation phase at specific retinal layer.

3. Results

3.1. Spatiotemporal characterization of IOSs with full and split OCT spectrums

The experimental data for this study were taken from Figure 3 of Zhang et al. (9) in which OCT images were collected with a frame rate of 100 Hz. B-scan images of 2 s pre-stimulation phase, and a 4 s post-stimulation phase including 10 ms light stimulation phase were reconstructed from the OCT signal. The OCT B-scan images were processed to obtain IOS images from full OCT spectrum and split OCT spectrums separately. Figure 1 shows the spatiotemporal characterization of functional OCT-IOS imaging from full OCT spectrum (Figure 1(a)) and split OCT spectrums (Figure 1(b1)–(b4)). The IOS images (Figure 1(b1)–(b4)) were calculated from sub-bands S1–S4, respectively. Stimulus onset is indicated by time '0'. All the images were averaged over 100 frames (1 s interval) to create IOS images. The IOS images show that IOSs predominantly distributed at the outer retina both in the full spectrum and split spectrums. Both positive and negative IOSs are consistently observed in full-band and sub-bands; however, the positions of IOSs may alter among different sub-bands. It was highly possible that the IOSs present at a point in S1 sub-band may be absent in other (S2–S4) sub-bands.

Since the localized IOSs can have different magnitudes among different sub-bands we took the absolute value of sub-band IOSs and combined them to yield a single IOS distribution map by using two methods: simple averaging and maximum projection. The absolute IOSs from the full-band and combined sub-band are shown in Figure 2. Figure 2(a) shows the spatiotemporal characterization of absolute IOS imaging from the full OCT spectrum. Figure 2(b) and (c) shows the combined absolute IOSs from the split OCT spectrums using simple averaging and maximum projection method, respectively. The visual inspection of the IOS images show that the magnitudes of IOSs in the combined sub-band OCT via maximum projection method were considerably larger than those of the full-band OCT and average sub-bands. Figure 2(d) shows number of activated pixels (positive and negative) from full-band and split-band OCT. The activated pixel number in split band OCT was computed in way that if an activated pixel is presented in one of the sub-band, then it will be counted. The results showed that the activated pixels were increased at least by twofold by calculating IOSs from multiple sub-bands and combining them by using a maximum projection method.

3.2. IOS from different layers of the retina

A differential M-scan tomogram (Figure 2(e) and (f)) provided more direct information about dynamic IOS changes in the individual functional layer over time. Every frame of the absolute IOS image was averaged towards the column direction and combined to generate a differential M-scan tomogram. The differential M-scan tomogram created by maximum projection of multiple sub-bands (Figure 2(f)) showed substantially higher IOS magnitudes in both outer and inner retina of the frog. It was observed that the stimulus-evoked changes occurred immediately after the stimulation in the outer retina in both full-band (Figure 2(e)) and sub-band (Figure 2(f)) OCTs. However, the changes are very small in the full-band OCT compared to the maximum projection of sub-band OCT. In addition, Figure 2(e) shows very small IOSs in the inner retina after few seconds of the stimulation onset. However, robust

IOSs occurred after few seconds of the stimulation in the inner retina with the combined sub-band (Figure 2(f)). Figure 2(g) shows temporal IOSs plotted from 3 different layers of the retina: (1) IPL indicated by dash lines in Figure 2(e), (2) OPL indicated by dash-dot lines in Figure 2(e) and (3) ISe + OS + RPE indicated by dash double-dot lines in Figure 2(e). In each layer, IOS from the full-band and split band OCTs were compared. In the outer retina (layer 3), fast IOSs were observed almost immediately after the stimulation onset; however, the plots indicate that split spectrum OCT generates significantly higher IOS magnitudes compared to the full spectrum. The IOSs in the inner retina (layers 1 and 2) were constantly increased after few seconds of the stimulation onset in the split spectrum OCT. In contrast, the IOSs from the full OCT spectrum were almost flat even after several seconds of the stimulation.

SNR from different layers of retina were also calculated to see the strength of the signal at each layer. IOS signals up to certain depth were averaged to create a signal at each retinal layer. The depths of each retinal layer are shown in Figure 2(e) and (f). The SNRs of IOS signals were calculated by using Eq. 8. The standard deviation was calculated from the pre-stimulation phase of the signal. The intensity of signal after 0.5 s was considered for calculating SNRs. Comparative SNRs from the full-band and split-band are shown in Figure 3. The SNRs from the split OCT spectrum were greater than those of the full OCT spectrum except for layer 1.

4. Discussion

In this study, we exploited split spectrum strategy to enhance the sensitivity of IOS recording from different layers of live frog retina. Although the axial resolution decreased with split spectrum OCT, resolution and quality of OCT structural images were sufficient for computing IOSs from different layers of the retina, as the OCT images reconstructed from split-bands properly showed individual retinal layers and structures (Figure 1(a)). It should be noted that there is a trade-off between a number of sub-bands and quality of the image; therefore we split the spectrum in such a way that the image quality does not degrade a lot. It can be seen in the IOS maps created from sub-band OCTs that the map from one sub-band is largely different from the maps of the other sub-bands (Figure 1(b1)–(b4)). The locations of positive and negative IOSs are not consistent among different sub-bands. It was also observed that the magnitude of IOS at a specific pixel location varies with spectral bands. As a matter of fact, if IOSs from different spectral bands were simply averaged, their magnitudes reduced or sometimes the responses completely wiped out. Therefore, it is reasonable to think that the IOSs obtained from full-band OCT were weaker because the intensity of backscattered light obtained from different spectra was already averaged that resulted weaker IOSs.

Differential M-scan tomograms created from full-band (Figure 2(e)) and split-band (Figure 2(f)) show more direct information about dynamic IOS changes in the individual functional layer over time. Comparative M-scan tomograms revealed a close correlation between the IOSs from the full-band and split-band OCTs. In the photoreceptor layer, the signal magnitude showed a rapid growth with the stimulus onset both in the full and split spectrum. Similarly, slow and low magnitude IOSs were observed in the inner retina with a delayed

time course (~2.5 s) Figure 2(g). There was no signal detected from the layers between IPL and OPL both in the full-band and split-band OCTs. Similarly, IOS signal was not detected from the layers between OPL and ISe. Furthermore, the widths of IOS maps of specific retinal layers were exactly equal in both full-band and split-band OCTs. The only difference between these two IOS maps was the difference in the magnitudes of IOSs, and SNRs. This indicates that the enhanced IOSs through the split spectrum strategy were not from artefacts. These truly represent the biophysical responses from various sources at different layers of the retina.

Although several studies have reported convincing IOSs, the sources of IOSs are still unclear. Zhang et al. (9) compared IOS maps and histological images of the outer retina to understand the anatomic sources of IOSs around the photoreceptor layer. Their results show that OS of photoreceptors are the primary source of IOSs in the outer retina, while they could not rule out the possibility of IOSs from ISe due to the changes at the inner and OS boundary during phototransduction. Occasionally observed IOSs at the RPE and choroidal layers are thought to be originated from microcirculation in the retinal capillaries (14). It is speculated that IOSs in the OS of the photoreceptor are related to the primary changes in the early stage of phototransduction. The IOSs can also be originated due to the secondary changes in the early stage of phototransduction such as cellular swelling or shrinking, produced by ion fluxes after the changes in the membrane polarization (14). Studies on isolated photoreceptors show transient photoreceptor displacement due to oblique (21, 22) or full or partial stimulation (23). It is highly possible that these trivial responses may wipe out upon averaging the responses from the large spectral band width. Split spectrum strategy computes IOSs from the small spectral band and fused them to a single map by using a maximum project method. The projection algorithm finds the maximum IOS for each pixel among the spectral bands, representing the highest spectral response. This might be a key factor for the difference in magnitude of the IOSs from the outer retina created from full-band and split-band OCTs. The IOSs in the inner retina; on the other hand, show delayed and low responses to the short stimulation. However, longer stimulation durations generate IOSs with greater magnitudes (9). This indicates that the observed IOSs in the inner retina were not artefacts but they correlated with the stimulus characteristics. The delayed IOS response in the inner retina is consistent with our early study of living retinal tissue (24). The difference in IOSs between the inner and outer retinal layers after the stimulation onset suggests that the physiological processes that occur in these layers are of different origin (14). Early studies show that the locations of the slow IOSs in the inner retina match with the locations of the retinal blood vessels. The backscattered light intensities change by moving particles, such as red blood cells in the flowing blood. Stimulus-evoked hemodynamic changes has been observed in individual retinal layers with different time courses (23). The contractions or relaxations of the arterioles are regulated by local neurons through the glial cells (25–27); therefore, microstructural changes of the blood vessel walls might cause possible changes in the intensity of the back scattered light. These trivial signals can be cancelled out upon spectral averaging. Although the exact reason cannot be confirmed from our current data but we speculate that the minor signals evoked from the microcirculation, activated neurons, and glial cells were the most likely preserved by the

split spectrum OCT. The minor signals which were absent in one spectral band were acquired from other spectral bands and did not cancel out by spectral averaging.

5. Conclusion

In summary, split spectrum OCT was used to enhance the sensitivity of IOS recording from the frog retina at subcellular resolution. The IOSs of individual sub-band OCTs were different and revealed different signal; the sensitivity of IOS recording can be improved by amalgamating IOSs from individual sub-band OCTs. The split spectrum technique reduces the correlation between the spectral bands; therefore, the subtle neural signals generated by a pixel can be enhanced. The proposed method resolves some of the challenges encountered by IOS imaging by improving the magnitude of IOS and SNR, which is essential for practical applications of functional IOS imaging. Further investigation is required to achieve an in-depth understanding of the IOS sources and mechanisms, which can provide insight for optimizing instrument design and stimulation protocols to improve IOS imaging sensitivity and selectivity.

Acknowledgments

Funding

This research was supported in part by NIH [grant number NIH R01 EY023522], [grant number NIH R01 EY024628], [grant number NSF CBET-1055889], [grant number NIH P30 EY001792].

References

1. Seiple WH, Siegel IM, Carr RE, Mayron C. Evaluating Macular Function Using the Focal ERG. Invest. Ophthalmol. Vis. Sci. 1986; 27(7):1123–1130. [PubMed: 3721790]
2. Vaegan, Billson F, Kemp S, Morgan M, Donnelley M, Montgomery P. Macular Electroretinograms: Their Accuracy Specificity and Implementation for Clinical Use. Aust. J. Ophthalmol. 1984; 12(4): 359–372. [PubMed: 6529380]
3. Yao X, Wang B. Intrinsic Optical Signal Imaging of Retinal Physiology: A Review. J. Biomed. Opt. 2015; 20(9):090901. [PubMed: 26405819]
4. Zhang QX, Zhang Y, Lu RW, Li YC, Pittler SJ, Kraft TW, Yao XC. Comparative Intrinsic Optical Signal Imaging of Wild-type and Mutant Mouse Retinas. Opt. Express. 2012; 20(7):7646–7654. [PubMed: 22453443]
5. Yao XC, Yamauchi A, Perry B, George JS. Rapid Optical Coherence Tomography and Recording Functional Scattering Changes from Activated Frog Retina. Appl. Opt. 2005; 44(11):2019–2023. [PubMed: 15835350]
6. Bizheva K, Pflug R, Hermann B, Považay B, Sattmann H, Qiu P, Anger E, Reitsamer H, Popov S, Taylor JR, Unterhuber A. Optophysiology: Depth- Resolved Probing of Retinal Physiology with Functional Ultrahigh-Resolution Optical Coherence Tomography. Proc. Nat. Acad. Sci. 2006; 103(13):5066–5071. [PubMed: 16551749]
7. Schmoll T, Kolbitsch C, Leitgeb RA. *In vivo* Functional Retinal Optical Coherence Tomography. J. Biomed. Opt. 2010; 15(4):041513. [PubMed: 20799791]
8. Srinivasan VJ, Wojtkowski M, Fujimoto JG, Duker JS. *In vivo* Measurement of Retinal Physiology with High-Speed Ultrahigh-Resolution Optical Coherence Tomography. Opt. Lett. 2006; 31(15): 2308–2310. [PubMed: 16832468]
9. Zhang Q, Lu R, Wang B, Messinger JD, Curcio CA, Yao X. Functional Optical Coherence Tomography Enables *in vivo* Physiological Assessment of Retinal Rod and Cone Photoreceptors. Sci. Rep. 2015; 5:9595. [PubMed: 25901915]

10. Wang B, Lu R, Zhang Q, Jiang Y, Yao X. En Face Optical Coherence Tomography of Transient Light Response at Photoreceptor Outer Segments in Living Frog Eyecup. Opt. Lett. 2013; 38(22): 4526–4529. [PubMed: 24322065]
11. Wang B, Lu Y, Yao X. *In vivo* Optical Coherence Tomography of Stimulus-Evoked Intrinsic Optical Signals in Mouse Retinas. J. Biomed. Opt. 2016; 21(9):096010.
12. Moayed AA, Hariri S, Choh V, Bizheva K. *In vivo* Imaging of Intrinsic Optical Signals in Chicken Retina with Functional Optical Coherence Tomography. Opt. Lett. 2011; 36(23):4575–4577. [PubMed: 22139247]
13. Moayed AA, Hariri S, Choh V, Bizheva K. Correlation of Visually Evoked Intrinsic Optical Signals and Electroretinograms Recorded from Chicken Retina with a Combined Functional Optical Coherence Tomography and Electroretinography System. J. Biomed. Opt. 2012; 17(1): 0160111–0160115.
14. Suzuki W, Tsunoda K, Hanazono G, Tanifuji M. Stimulus-induced Changes of Reflectivity Detected by Optical Coherence Tomography in Macaque Retina. Invest. Ophthalmol. Vis. Sci. 2013; 54(9):6345–6354. [PubMed: 23982841]
15. Srinivasan VJ, Chen Y, Duker JS, Fujimoto JG. *In vivo* Functional Imaging of Intrinsic Scattering Changes in the Human Retina with High-speed Ultrahigh Resolution OCT. Opt. Express. 2009; 17(5):3861–3877. [PubMed: 19259228]
16. Hillmann D, Spahr H, Pfäffle C, Sudkamp H, Franke G, Hüttmann G. *In vivo* Optical Imaging of Physiological Responses to Photostimulation in Human Photoreceptors. Proc. Nat. Acad. Sci. 2016; 113(46):13138–13143. [PubMed: 27729536]
17. Jia Y, Tan O, Tokayer J, Potsaid B, Wang Y, Liu JJ, Kraus MF, Subhash H, Fujimoto JG, Hornegger J, Huang D. Split-spectrum Amplitude-decorrelation Angiography with Optical Coherence Tomography. Opt. Express. 2012; 20(4):4710–4725. [PubMed: 22418228]
18. Li YG, Zhang QX, Liu L, Amthor FR, Yao XC. High Spatiotemporal Resolution Imaging of Fast Intrinsic Optical Signals Activated by Retinal Flicker Stimulation. Opt. Express. 2010; 18(7): 7210–7218. [PubMed: 20389742]
19. Yao XC, Liu L, Li YG. Intrinsic Optical Signal Imaging of Retinal Activity in Frog Eye. J. Innovative. Opt. Health. Sci. 2009; 02(2):201–208.
20. Wojtkowski M, Srinivasan VJ, Ko TH, Fujimoto JG, Kowalczyk A, Duker JS. Ultrahigh-resolution, High-speed, Fourier Domain Optical Coherence Tomography and Methods for Dispersion Compensation. Opt. Express. 2004; 12(11):2404–2422. [PubMed: 19475077]
21. Lu R, Levy AM, Zhang Q, Pittler SJ, Yao X. Dynamic near-Infrared Imaging Reveals Transient Phototropic Change in Retinal Rod Photoreceptors. J. Biomed. Opt. 2013; 18(10):106013. [PubMed: 24165739]
22. Wang B, Zhang Q, Lu R, Zhi Y, Yao X. Functional Optical Coherence Tomography Reveals Transient Phototropic Change of Photoreceptor Outer Segments. Opt. Lett. 2014; 39(24):6923–6926. [PubMed: 25503031]
23. Son T, Wang B, Thapa D, Lu Y, Chen Y, Cao D, Yao X. Optical Coherence Tomography Angiography of Stimulus Evoked Hemodynamic Responses in Individual Retinal Layers. Biomed. Opt. Express. 2016; 7(8):3151–3162. [PubMed: 27570706]
24. Li YC, Strang C, Amthor FR, Liu L, Li YG, Zhang QX, Keyser K, Yao XC. Parallel Optical Monitoring of Visual Signal Propagation from the Photoreceptors to the Inner Retina Layers. Opt. Lett. 2010; 35(11):1810–1812. [PubMed: 20517424]
25. Kotliar KE, Vilser W, Nagel E, Lanzl IM. Retinal Vessel Reaction in Response to Chromatic Flickering Light. Graefe's Arch. Clin. Exp. Ophthalmol. 2004; 242(5):377–392. [PubMed: 14770317]
26. Metea MR, Newman EA. Glial Cells Dilate and Constrict Blood Vessels: A Mechanism of Neurovascular Coupling. J. Neurosci. 2006; 26(11):2862–2870. [PubMed: 16540563]
27. Newman EA. Calcium Increases in Retinal Glial Cells Evoked by Light-induced Neuronal Activity. J. Neurosci. 2005; 25(23):5502–5510. [PubMed: 15944378]

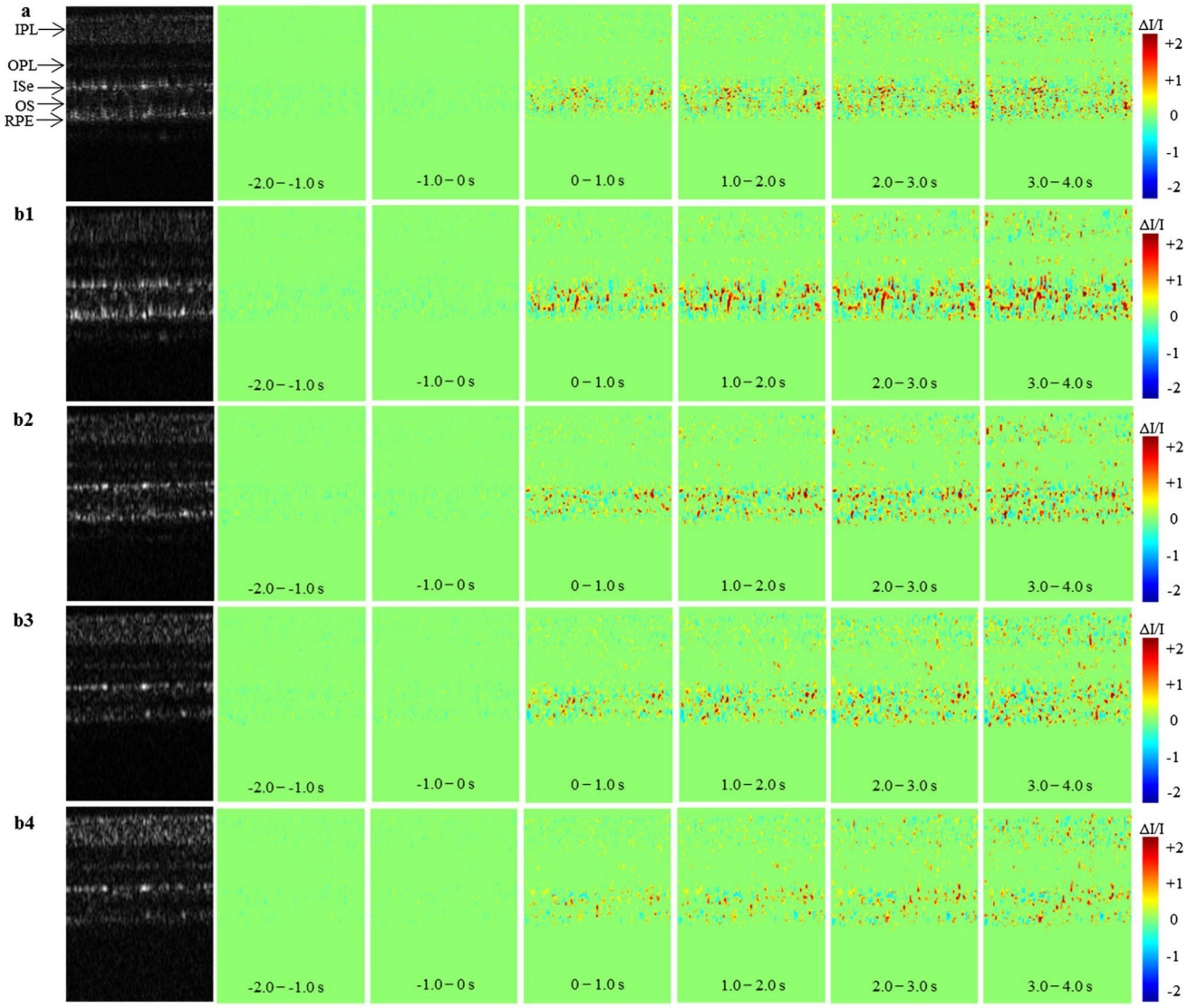

Figure 1.

The spatiotemporal characterization of functional OCT -IOS imaging with a 10 ms flash stimulus.

Notes: The data were taken from Figure 3 of Zhang et al. (9) in which OCT images were collected with a frame rate of 100 Hz. Stimulus onset is indicated by time '0'. (a) OCT B-scan images and spatial IOS image sequences of full-band OCT. (b1–b4) OCT B-scan images and spatial IOS image sequences of sub-band S1–S4. All the images were averaged over 100 frames (1 s interval) to generate IOS images. IPL: inner plexiform layer, OPL: outer plexiform layer, ISe: inner segment ellipsoid, RPE: retinal pigment epithelium.

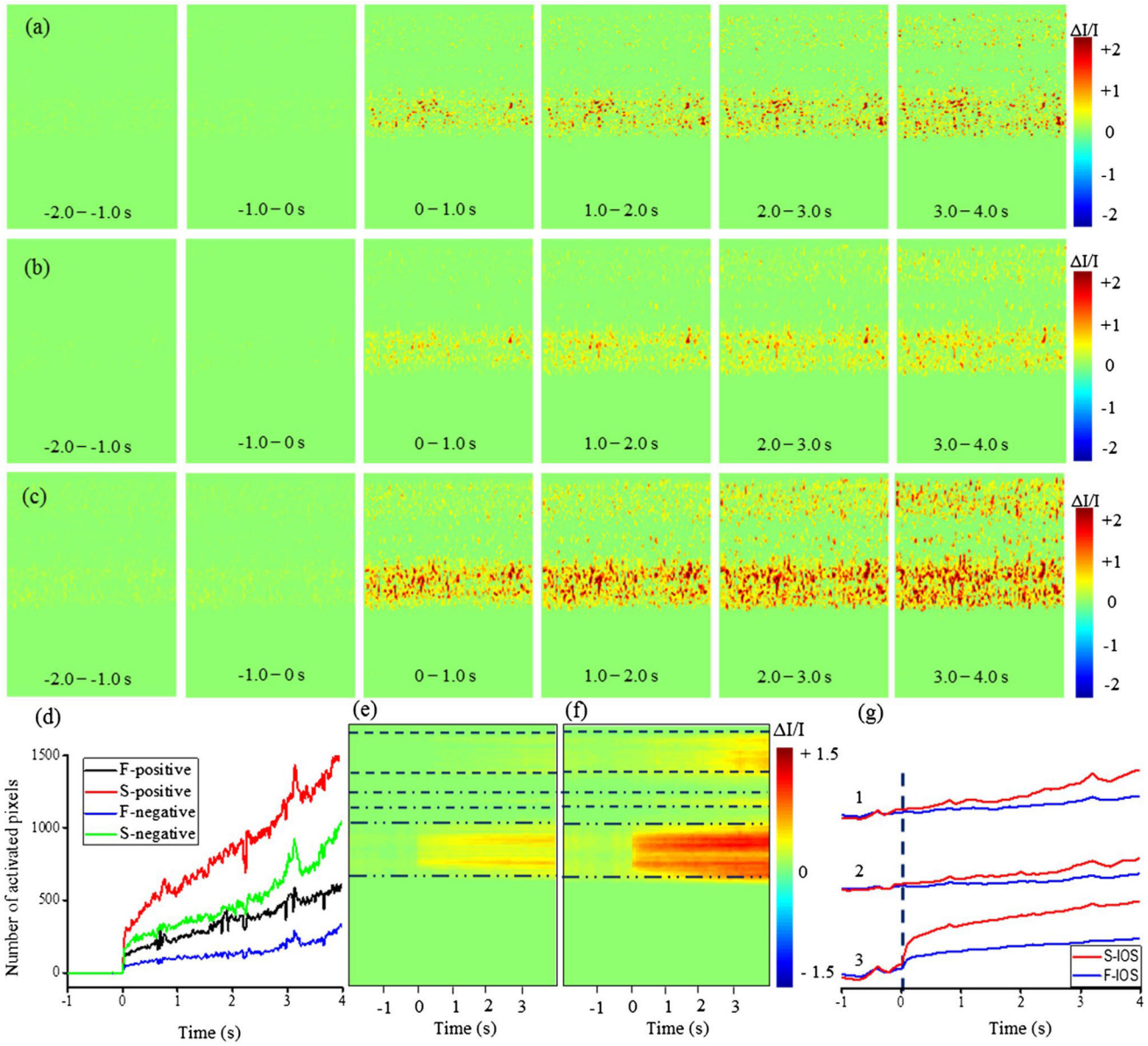

Figure 2.

The spatiotemporal characterization of functional OCT -IOS imaging with a 10 ms stimulus. Notes: the data were taken from Figure 3 of Zhang et al. (9) in which OCT images were collected with a frame rate of 100 Hz. Stimulus onset is indicated by time “0”. (a) Absolute spatial IOS image sequences of full-band OCT. (b) Average absolute spatial IOS image sequences of sub-bands. (c) Absolute spatial IOS image sequences of combined sub-bands with maximum projection method. (d) Temporal curves of the number of activated pixels (F = full and S = split) in full OCT and split OCT spectrums. (e) Differential M-scan tomogram created from full OCT spectrum of panel (a). (f) Differential M-scan tomogram created from split OCT spectrum of panel (c). (g) Comparative temporal IOSs between full-band (F-IOS) and split-band (S-IOS) at different layers of the retina, (1) IPL indicated by dash lines in e

and f, (2) OPL indicated by dash-dot lines in (e) and (f), and (3) outer retina (ISe + OS + RPE) indicated by dash double-dot lines in e and f.

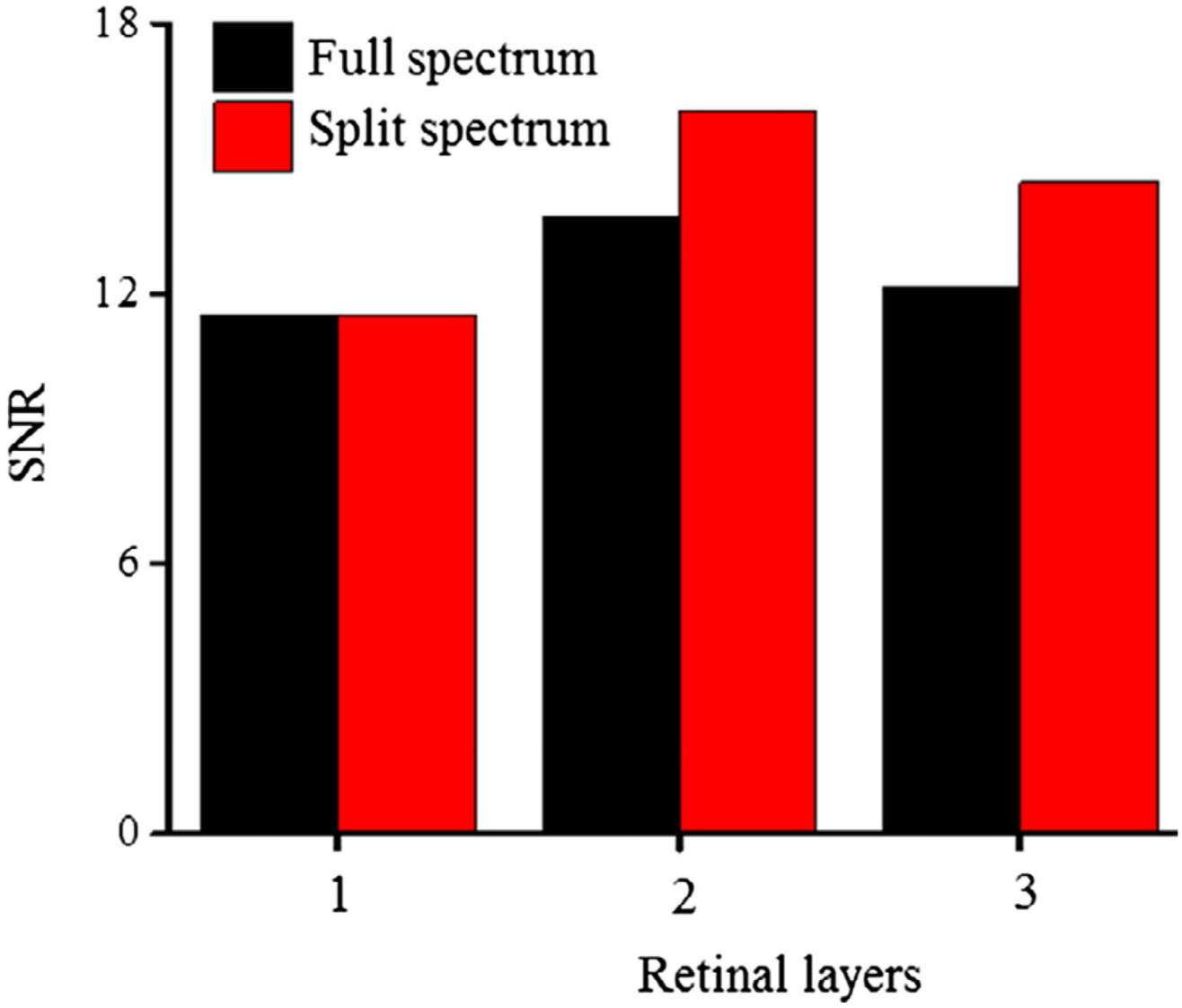

Figure 3.

Comparison of SNRs between full OCT spectrum and Split OCT spectrum at different layers of the retina: (1) IPL indicated by dash lines in Figure 2(e) and (f), (2) OPL indicated by dash-dot lines in Figure 2(e) and (f), and (3) outer retina (ISe + OS + RPE) indicated by dash double-dot lines in Figure 2(e) and (f).